Smart Packaging: A micro-sensor array integrated to a flip-chip package to investigate the effect of humidity in microelectronics package

Aurore Quelennec, Hélène Frémont
Université de Bordeaux
IMS, UMR 5218
Bordeaux, France
aurore.quelennec@u-bordeaux.fr

Aurore Quelennec, Umar Shafique, Dominique Drouin
Institut Interdisciplinaire d'Innovation Technologique (3IT),
Laboratoire Nanotechnologies Nanosystemes (LN2)
- CNRS UMI-3463,
Université de Sherbrooke,
3000 Boul. Université,
Sherbrooke, J1K 0A5, QC, Canada
aurore.quelennec@usherbrooke.ca

Éric Duchesne
IBM Canada Ltd,
23 Boul. de l'Aéroport,
Bromont, J2L 1A3,
QC, Canada
educhesn@ca.ibm.com

***Abstract*—Lifetime reliability of electronics package is important for long term operation of microelectronic devices. Humidity, temperature and resulting strain are three main reasons for the failure of a flip-chip semiconductor package. For these reasons, continuous research effort have been devoted to integrate moisture, temperature and strain sensors in package performance and failure risk monitoring. We here demonstrate combined humidity, strain and temperature sensors based on a carbon nanotube mesh embedded in a polyimide matrix. We further demonstrate that an array of micro-humidity(/strain/temperature) sensors can be integrated at the wafer finish step of semiconductor chips to provide useful *in-situ* real-time information.**

***Keywords*-Carbon nanotubes sensors; moisture; strain; temperature; reliability; flip-chip devices;**

I. Introduction

In high-performance semiconductors, the back-end-of-line (BEOL) interconnect pitch has been shrinking for decades following Moore's law. Steady advances in very-large-scale integration (VLSI) technology for both digital and analog devices could never have been achieved without overcoming various reliability risks in integrated circuit (IC) chips as well as in packages. In many cases, such challenges do not reside solely in a package or an IC chip. Rather, the interaction between the package and the IC chip is important as the coefficients of thermal expansion (CTEs) of the silicon die and package materials, such as plastic molding compounds or organic substrates, can differ significantly. This CTE mismatch induces thermo-mechanical stresses at the interfaces during thermal excursions, which can compromise the chip's structural integrity. The influence of the package-induced stress [1] on the chip is called chip-package interaction (CPI), and it plays a key role in overall product reliability. Similarly, moisture absorption by the different materials used can cause delamination and/or corrosion, which can also affect overall product reliability. In order to identify the impact of humidity and temperature in a flip-chip package, previous investigation techniques used by the industry such as destructive mass spectroscopic analysis were complex and unable to deliver *in situ* and in real-time information about the package defects and failure mechanisms.

To integrate sensors in the flip-chip package and get real time *in situ* measurements, well established technologies like silicon-based piezoresistive [2] or metal foil-based [3] as strain sensors, aluminium oxide-based [4] or polyimide-based [5] as humidity sensors and transistors or diodes as temperature sensors are commonly used by the industry. However, disadvantages like their size, low sensitivity, lack of positioning flexibility and/or their incompatibility with existing micro-electronic processes limit their use. For instance, these sensors cannot be placed close to or under critical chip structures like ball limiting metallurgy (BLM) or on the passivation layer between flip chip interconnects. Moreover, most of them are integrated at the silicon level taking area used for CMOS and adding complexity in the design process. Thus, these common sensors cannot be retrofit on an existing product.

More recently, carbon nanotube/polyimide composite-based sensors have been introduced and represent a promising alternative for humidity [6], [7], strain [8]–[10] and temperature [11] sensors. This work will demonstrate that these sensors can be integrate after the wafer fabrication and before the assembly process, using common UV-lithography and spray-coating techniques. We will show that these sensors are highly sensitive to strain, temperature or humidity. Moreover, these sensors can be organized as an array on the passivation layer of the chip, in order to get the trinomial vector (T, ϵ, RH) real-time distribution, where T is the temperature, ϵ the strain, and RH the relative humidity. This data can be used to ease the fundamental understanding of various packaging defects and failure mechanisms. Such data can also help

2377-5726/17 $31.00 © 2017 IEEE
DOI 10.1109/ECTC.2017.140

to optimize the package design, the assembly and the test processes. Furthermore, those sensors can be added to the package for in-field performance and failure risk monitoring.

This article is structured in to four parts. The first one address the prototype fabrication, the second one the characterization of the test sensors and the third one the integration of the sensors within a test vehicle. Finally, the fourth part presents the results of the integration process.

II. Prototype Fabrication

A cleaned 520 μm thick (e_p) silicon wafer is used, to mimic a typical chip. The process steps are the following ones : a polyimide HD4104 layer is spin coated on the wafer and cured at 200 ^oC for 30 min followed by a curing at 375 ^oC for 60 min resulting in a 3 μm thickness.

Multiwall carbon nanotubes, previously functionalized with carboxyl groups (COOH-MWCNT), are dispersed in a N-Methyl-2-pyrrolidone solvent (NMP) with a ratio of 1 mg/10 mL, using ultrasound for 20 min. The carbon nanotube solution is spray coated on the polyimide surface to cover the wafer. During this step, the wafer is placed on a hot plate at 220 ^oC in order to evaporate the solvent. The thickness of the carbon nanotube mesh deposited can vary between 400 nm to 700 nm.

As shown in figure 1, the sensor prototype is composed of two passive component patterns, a meander and a rectangular patch characterized by specific geometric parameters. The sensor design is defined using a UV lithography step. A positive resist is used to pattern and protect the carbon nanotubes to be kept. With an oxygen based plasma reactive ion etching step, the unprotected carbon nanotubes are removed. The positive resist is then stripped with immersion in acetone for 5 min, then cleaned into isopropanol for 5 min and DI water for 5 min.

The carbon nanotubes mesh is then encapsulated with HD4104 polyimide and contact opening to the sensor is done using UV lithography step. The polyimide is then cured in a furnace.

A 700 nm layer of titanium, or titanium tungsten, compatible with CNT's is used as contact electrodes, in order to provide an adequate electrical contacts to the passive sensor [12]. The metal layer has to be thicker than the COOH-MWCNT layer in order to get non-rectifying electrical contact. For these tests vehicules, the electrodes are covered with a 150 nm layer of gold to avoid any oxidation of the contact surface. Figure 2 associated with table I resumes the fabrication steps of the prototype and figure 3 shows an optical microscope picture of a prototype sensor.

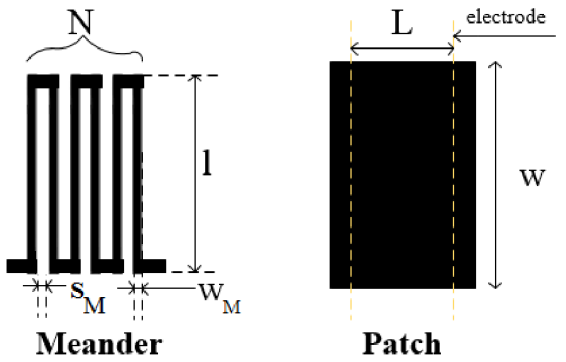

Figure 1: Sensors geometries and parameters definition.

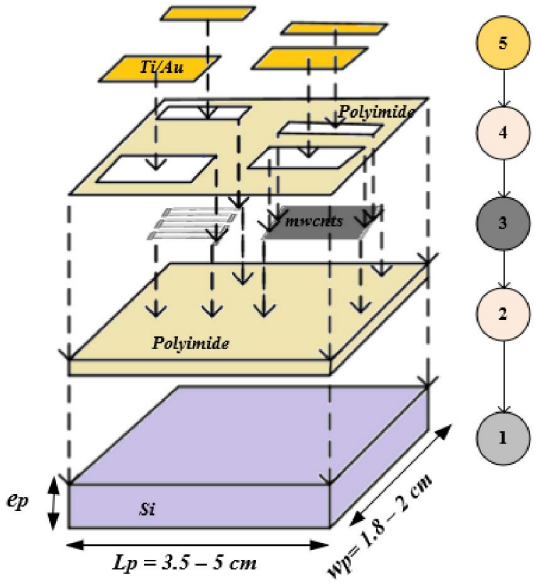

Figure 2: Integration process flow showing the principal fabrication steps of the sensors prototype.

Table I: Summary of the process fabrication steps.

Step	Materials	Thickness	Objective
1	Silicon	520 μm	Chip
1.5	Si_3N_4	200 nm	Isolation
2	Polyimide	3 μm	Passivation layer
2.5	Aluminium	300 nm	Conductor layer BLM to sensors
3	Carbon nanotubes	400-700 nm	Sensors
4	Polyimide	3 μm	Protective layer
5	Ti or TiW + Au	700 nm + 150 nm	Contact pads
6	Polyimide	3 μm	Isolation

III. Characterization

Before integration the sensors on a test vehicle chip, prototype sensors are fabricated using the process describe in section II and characterized individually.

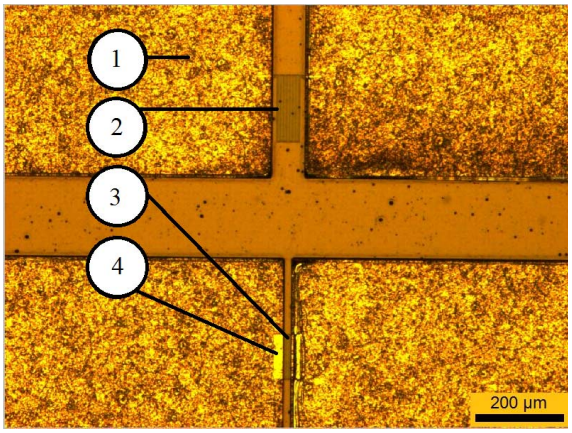

Figure 3: Optical microscope picture of the fabricated prototype. (1) is the electrode, (2) the meander part of the sensor, (3) the patch part of the sensor, (4) the connection area between carbon nanotubes and contact electrode.

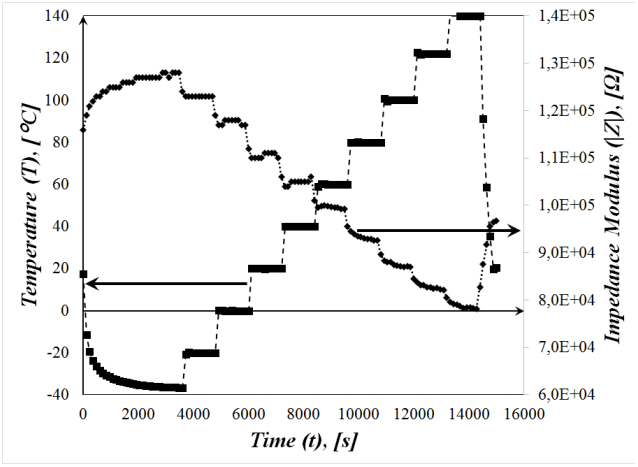

Figure 4: Graphics showing the temperature applied as a function of time and the impedance modulus measured at 1 kHz of a patch sensor.

The ohmic contact quality is first tested using a four-point probe. Then, cables are added to connect the sensor contact pads to coaxial cables. The response of each sensor to humidity, strain or temperature is characterized by the impedance modulus ($|\underline{Z}|$) of the sensor. The response is measured with an impedance analyser Keysight E4990A.

A. Temperature measurement

The sensor is placed into a Climats Excal 1411-HE chamber in which the air temperature of the air applied is increased by steps from -40 ^oC to 140 ^oC. A polyimide test board resistant to high temperature is used to connect wires from the sensor to coaxial cables also resistant to high temperatures (figure 6). Careful attention is taken not to induce any stress to the sensors during this experiment. The sensor response is observed by increasing the temperature by 20 ^oC every 20 min (figure 4). As we can observe on figure 4, the impedance modulus of the sensor follows the temperature change in the chamber.

B. Humidity measurement

Using the same setup, the relative humidity is increased in steps from 30 %RH to 100 %RH at 25 ^oC. The sensor placed in the chamber is stress-free, as for temperature measurements. The response of the impedance is observed by increasing the relative humidity by 10 % every 20 min (figure 5). As shown figure 5, the impedance modulus of the sensor follows the change of the ambient humidity in the chamber.

C. Low strain measurement

The sensor strain response is evaluated using an Instron 5565 four-point bend test setup as shown on figure 6. The prototype is placed face down between the upper and bottom fulcrum at the center of the fixture (figures 6 and 7). During the test, the sensor is under an ambient temperature of 25 ^oC and a humidity of 40-50 %RH. A force (F) is applied on the sensor prototype silicon substrate face from 0.1 N to 10 N using a ramp with a speed of $0.04\ N/s$ (figure 8). The strain (ϵ) is calculated using equation 1, where w_p = 1.8 to 2 cm is the prototype width (figure 2), and e_p = 520 μm the prototype thickness. For the range of forces applied, the strain varies from 0 to 400 ppm. Again as shown on figure 8, the impedance modulus of the sensor follows the change in strains applied to the sensor.

$$\epsilon = \frac{3F(L_f - l_f)}{2Ew_p e_p^2} \quad (1)$$

IV. Integration on chip

Figure 9 shows the proposed integrations scheme of 100 sensors disposed in array on a 2 cm x 2 cm chip. For each coordinates (X_i, Y_j), the trinomial vector (T, RH, ϵ) can be extracted.

The fabrication process of such a test vehicle is very similar to that of prototypes described in the section II but with three additional steps (figure 10 and table I). Firstly a 200 nm silicon nitride layer is added between the bare silicon wafer and the polyimide layer to mimic a typical integrated circuit final passivation layer. Secondly, before the carbon nanotubes spray coating step, aluminium interconnection lines are patterned between the contact pads of the sensors and the chip BLM's, with a standard photolithography and metal etch process. A final passivation layer using HD4104 polyimide is used to electrically isolate the contact pads. In this example, the sensors can be externally probe via

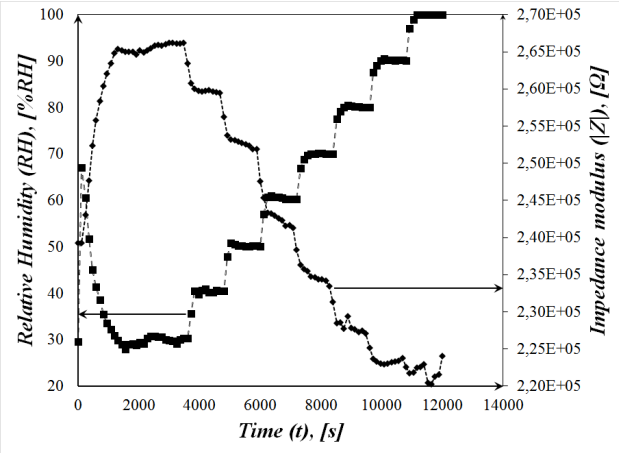

Figure 5: Graphics showing the relative humidity applied as a function of time and the impedance modulus at 1 kHz of a meander sensor.

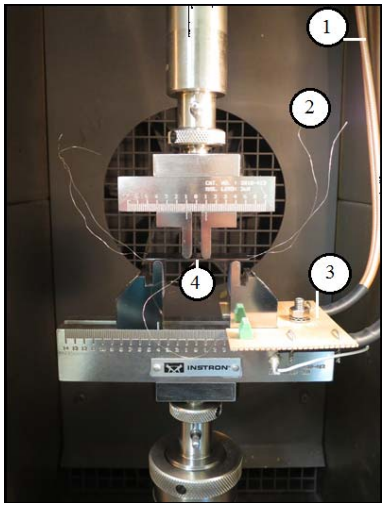

Figure 6: Picture of the four-point bend test. (1) coaxial cables, (2) sensor's wires, (3) test board, (4) prototype.

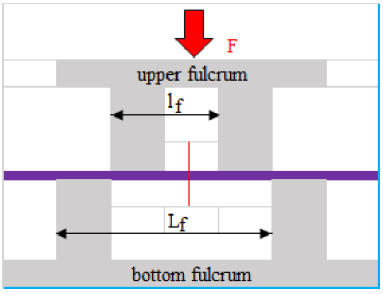

Figure 7: Schematic of the four-point bend test. L distance between the two bottom fulcrums, l distance between the two top fulcrums.

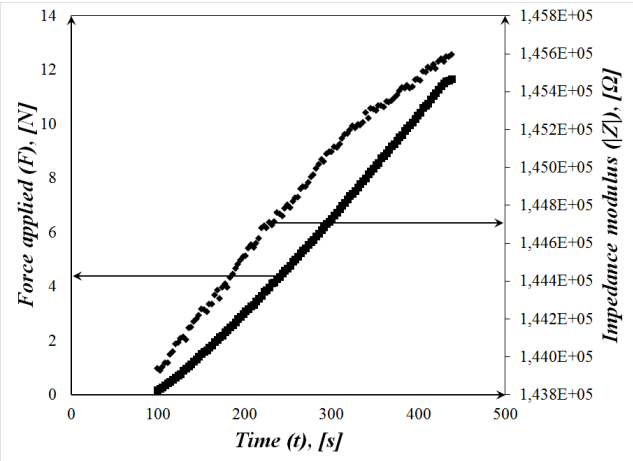

Figure 8: Graphics showing the force applied as a function of time and the impedance modulus measured at 10 kHz of a meander sensor.

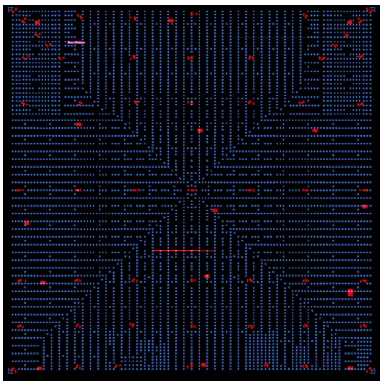

Figure 9: Sensors placement on the chip in order to get for each emplacement (T, RH, ϵ).

available C4-BGA nets on the laminate side after final assembly. Figure 11 shows an optical microscope picture of an integrated meander and patch sensor with their respective aluminum interconnection lines and titanium contact pads. The latest provide compatibility and adequate electrical contact between the carbon nanotubes and the aluminum interconnection lines.

V. Results

Figures 12 to 14 present the temperature, humidity and strain responses of a patch and meander sensor. The patch sensor geometry is 10 μm length (L), 100 μm width (w) and 400 to 700 nm thick (e_p). For the meander, the dimensions are 150 μm length (l), 4 bridges (N), 4 μm width (w_M), 2 μm line space (s_M), and 400 to 700 nm thick (e_p).

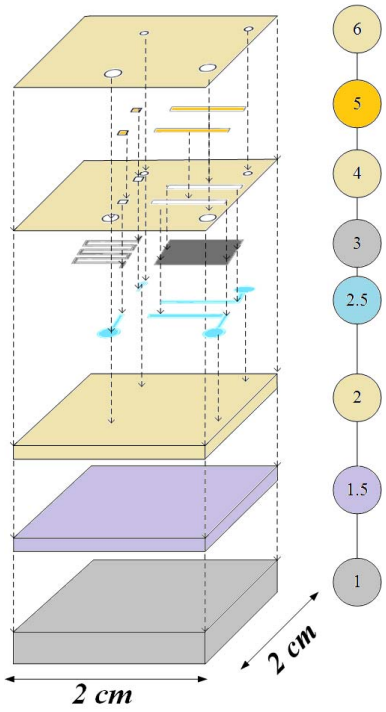

Figure 10: Schematic showing the steps of the sensors within the test vehicle.

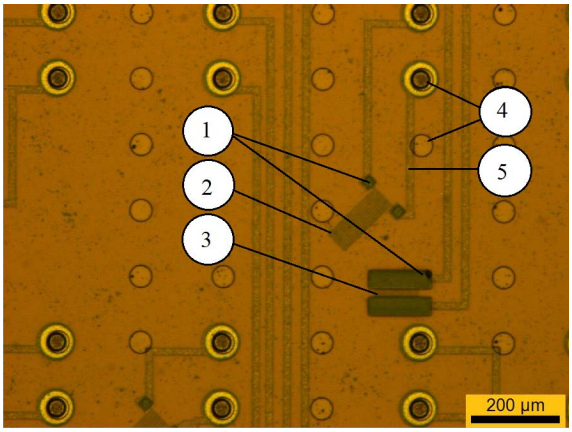

Figure 11: Microscope picture of an integrated sensor at the final step. (1) contact pads in titanium, (2) meander, (3) patch, (4) examples of BLM openings in polyimide and (5) aluminium connection.

A. Temperature measurements

Figure 12 shows the temperature response of the patch sensor measured at a frequency of 1 kHz. As the temperature response is linear, the sensitivity s_T can be defined as the ratio of the variation of the impedance modulus and the variation of temperature (equation 2). The sensitivity of the temperature sensor is -290 $\Omega/^oC$, and $|\underline{Z}(T_{min})| = 128\ k\Omega$

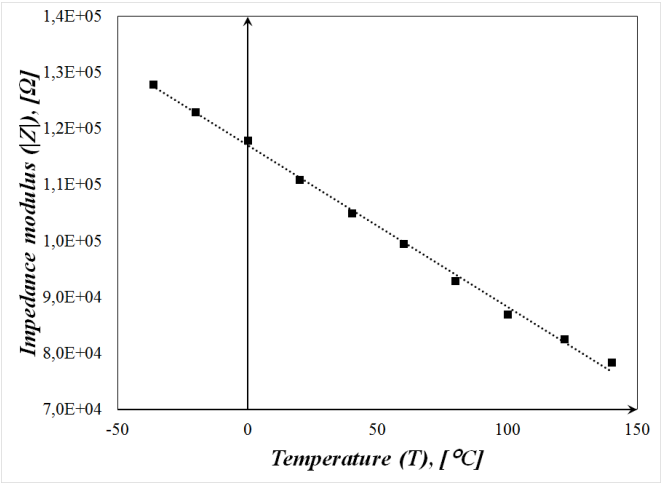

Figure 12: Impedance modulus measured at 1 kHz of the patch sensor as a function of the temperature.

with $T_{min} = -36\ ^oC$.

$$s_T = \frac{|\underline{Z}(T_{max})| - |\underline{Z}(T_{min})|}{\Delta T} \tag{2}$$

B. Humidity measurements

Figure 13 shows the humidity response of the meander sensor measured at a frequency of 1 kHz. As for the temperature response, the humidity response is linear and the sensitivity to moisture of the sensor with regards to humidity, s_{RH}, as defined by equation 3, is -696 $\Omega/\%RH$, where $|\underline{Z}(RH_{min})| = 266\ k\Omega$ and $RH_{min} = 30\ \%$.

$$s_{RH} = \frac{|\underline{Z}(RH_{max})| - |\underline{Z}(RH_{min})|}{\Delta\%RH} \tag{3}$$

C. Strain measurements

Figure 14 shows the strain response of the meander sensor measured at a frequency of 2 kHz. The response is linear over the entire strain range of 0 to 500 ppm. The sensitivity of the strain gauge s_ϵ can be defined as the ratio of relative change in impedance to the mechanical strain (equation 4). The sensitivity of the strain sensor is 25 for strains below 500 ppm.

$$s_\epsilon = \frac{|\underline{Z}(\epsilon_{max})| - |\underline{Z}(\epsilon_{min})|}{|\underline{Z}(\epsilon_{min})|} \frac{1}{\Delta\epsilon} \tag{4}$$

The proposed sensor allows to measure the strain, relative humidity and temperature with the same sensor. A simple signal treatment is required to decouple the different responses, and hence, to have (ϵ, RH, T) at a given position of a chip.

Four prototypes were tested within the framework of this study. As expected for a prototyping phase, there is a dispersion in the sensors impedance modulus (at ambient conditions and no charge applied) and the sensor sensitivity.

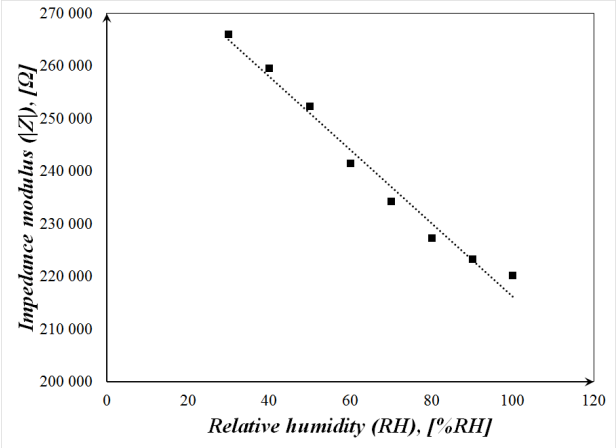

Figure 13: Impedance modulus measured at 1 kHz of the meander sensor as a function of the relative humidity.

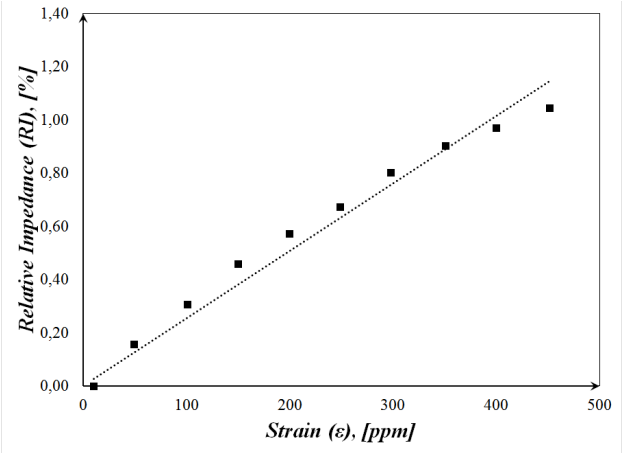

Figure 14: Relative change in impedance modulus measured at 2 kHz of the meander sensor as a function of the strain.

However, for each sensor, the behavior described above is the same. This dispersion may be attributed to a variation in the density of carbon nanotubes in the fabricated sensors. It is envisioned, that a transition from prototyping to mass production will provide a more reproducible process, which will reduce such dispersion. However, an initial calibration step of the sensors is recommended.

In order to compare our prototypes with current technologies, we used the normalized sensitivity as presented in equation 4. Table II presents the normalized sensitivity of the proposed sensors to humidity -4 x $10^{-3}/\%RH$, temperature sensor -2.5 x $10^{-3}/^{o}C$ and strain gauge 25 for low strain values below 500 ppm. Table II compares the normalized sensitivity of different sensor technologies from the literature

Table II: Normalized sensitivity comparison of different sensors technologies [3], [5], [13].

Technology	$s_{T,n}$ $[10^{-3}/^{o}C]$	$s_{RH,n}$ $[10^{-3}/\%RH]$	s_{ϵ}
Diodes	2 to 3		
Polyimide		1.8	
Si-based piezoresistive			150 to 200
Foil-based			2 to 4
Proposed sensor	-2.5	-4	25

with the proposed sensors. The proposed sensors based on carbon nanotubes embedded in polyimide provide a better or similar sensitivity to alternate technologies with the clear advantage of ease of integration at the packaging level.

VI. Conclusion

We proposed in this work a fabrication process for highly sensitive sensors to strains, to humidity and to temperature. A sensitivity greater than 25 for extremely low strains value below 500 ppm has been demonstrated. For humidity and temperature a sensitivity of $-696\ \Omega/\%RH$ and $-290\ \Omega/^{o}C$, respectively, have been shown. These sensitivities are in the range of best sensors based on literature. Furthermore, our technology allows to measure the strain, relative humidity and temperature with the same sensor using simple signal treatment to decouple the different responses, and hence, to have (ϵ, RH, T) at a given position of a chip. The fabrication process is compatible with existing wafer back-end-of-line (BEOL) processing and the resulting sensors are adapted to temperatures, humidity and strain measurements in the packaging assembly process and reliability testing environments. We succeeded with the integration of the sensors on a test vehicle chip. This chip will be integrated in future work into a package enabling thorough *in situ* stress and moisture absorption-desorption studies during bond and assembly and reliability testing.

Acknowledgment

We would like to thank our trainee student Ariane Tomas for her help during the fabrication, and, the several organizations (IBM, NSERC, MESR France) which finance this research.

References

[1] E. H. Wong and T. B. Lim, "A more comprehensive solution for tri-material layers subjected to thermal stress," *IEEE Transactions on Components and Packaging Technologies*, vol. 31, no. 1, pp. 54–64, March 2008.

[2] J. C. Suhling and R. C. Jaeger, "Silicon piezoresistive stress sensors and their application in electronic packaging," *IEEE Sensors Journal*, vol. 1, no. 1, pp. 14–30, June 2001.

[3] T. Kieffer, R. Watson, and S. Harris, "Foil strain gage for automated handling and packaging," Dec. 19 2006, uS Patent 7,150,199. [Online]. Available: http://www.google.ch/patents/US7150199

[4] R. R. Tummala, E. J. Rymaszewski, and A. G. Klopfenstein, "Microelectronic packaging handbook : semiconductor packaging, part ii second edition," *Springer Science + Business Media New York*, pp. 913 – 915, 1997.

[5] M. Dokmeci and K. Najafi, "A high-sensitivity polyimide capacitive relative humidity sensor for monitoring anodically bonded hermetic micropackages," *Journal of Microelectromechanical Systems*, vol. 10, no. 2, pp. 197–204, Jun 2001.

[6] W.-P. Chen, Z.-G. Zhao, X.-W. Liu, Z.-X. Zhang, and C.-G. Suo, "A capacitive humidity sensor based on multi-wall carbon nanotubes (mwcnts)," *Sensors (Basel)*, vol. 9, pp. 7431–7444, 2009.

[7] C. L. Cao, C. G. Hu, L. Fang, S. X. Wang, Y. S. Tian, and C. Y. Pan, "Humidity sensor based on multi-walled carbon nanotube thin films," *Journal of Nanomaterials*, vol. 2011, p. 5, 2011.

[8] W. Obitayo and T. Liu, "A review: Carbon nanotube-based piezoresistive strain sensors," *Journal of Sensors*, vol. 2012, p. 15, 2012.

[9] D. Lee, H. P. Hong, C. J. Lee, C. W. Park, and N. K. Min, "Microfabrication and characterization of spray-coated single-wall carbon nanotube film strain gauges," *Nanotechnology*, vol. 22, no. 45, 2011.

[10] J. Genest and J. Beauvais, "Spray coating carbon nanotube thin films on flexible substrates for stress and strain monitoring systems," *Nanotechnologies and Nanosystems Laboratory (LN2) – CNRS, Sherbrooke*, 2014. [Online]. Available: http://csstc2015.ca/wp-content/uploads/2014/03/GENEST_J_c23.pdf

[11] K. S. Karimov, M. T. S. Chani, and F. A. Khalid, "Carbon nanotubes film based temperature sensors," *Physica E: Low-dimensional Systems and Nanostructures*, vol. 43, no. 9, pp. 1701 – 1703, 2011. [Online]. Available: http://www.sciencedirect.com/science/article/pii/S1386947711001950

[12] S. C. Lim, J. H. Jang, D. J. Bae, G. H. Han, S. Lee, I.-S. Yeo, and Y. H. Lee, "Contact resistance between metal and carbon nanotube interconnects: Effect of work function and wettability," *Applied Physics Letters*, vol. 95, no. 26, 2009. [Online]. Available: http://scitation.aip.org/content/aip/journal/apl/95/26/10.1063/1.3255016

[13] J. Schwizer, M. Mayer, and O. Brand, *Force Sensors for Microelectronic Packaging Applications*. Springer Science + Business Media, 2006.